Plasmonics (2021) 16:2061–2071
https://doi.org/10.1007/s11468-021-01465-y

Metamaterial Microwave Absorber (MMA) for Electromagnetic Interference (EMI) Shielding in X-Band

Ramesh Kumar Mishra[1] · Ravi Dutt Gupta[2] · Suwarna Datar[1]

Received: 17 March 2021 / Accepted: 17 May 2021 / Published online: 26 May 2021

Abstract

The present paper is aimed at investigating application of planar metamaterial (MM) structures for effective EMI shielding and stealth capability in X-Band. Various MM structures using FR-4 substrate and copper conductors were conceived and designed followed by simulations carried out using CST MWS Suite software. As a first step, the designs were aimed at achieving extremely high absorption for normal incidence, polarisation independence and maintaining high absorption in wide-angle performance while keeping the requirement of light weight, flexibility and environmental ruggedness in mind for deployability on platforms to achieve effective stealth capability against radars and for other EMI shielding applications. Circularly symmetric, single layer Metamaterial Microwave Absorber (MMA) design over thin FR-4 substrate in spokes and wheel structural arrangement provided these desired features. The thin FR4 substrate of 0.6 mm provides the light weight and flexibility while absorbing the EM waves. Rotational symmetry of the spoke and cut-wheel design gives it polarisation independence and 4 ring planar array concept with rings scaled to different sizes in the same plane in the unit cell provided the increase in bandwidth. Reduction in received signal level of the echo is depicted by the S-parameter at the input port. Getting values of this S-parameter less than -60 dB at resonant frequency for MMAs is highly encouraging and is not reported much in literature. Enhancement of nearly 3-8 times in operating bandwidth was achieved by changing size of rings in each quadrant in the co-planar array having four resonant rings in each unit cell.

Keywords Metamaterial · Rotational symmetry · Microwave absorber · EMI shielding

Introduction

The concept of negative refractive index was introduced by Vaselago in his seminal article [1] which was realised by using metallic wires and split-ring resonators to separately demonstrate negative permittivity and negative permeability materials, respectively, in the 1990s by Pendry et al. [2] Later, Smith et al. experimentally realised these structures in the microwave regime by using both the structures simultaneously in specific ways to produce Left Handed Materials (LHMs). [3] Such materials have unique properties which depend on the "meta atomic structure", rather than the materials they are made up of. Since the introduction of concept of LHMs, many applications of metamaterials like invisibility cloaks, [4, 5] super-lens, [6] antennas, [3] electromagnetic (EM) wave absorbers, [7] and so on, have been investigated.

With development and use of electronics in every area of life, there is always a need for Radar Absorbing Material (RAM) for applications such as Electromagnetic Interference (EMI) shielding, Electromagnetic Compatibility (EMC), communication antennas, stealth capability, etc. Researchers are working on RAM to improve their performance in absorption, the absorption bandwidth, polarisation and angle of incidence independence, etc. [8, 9]. Extensive research has been done in the area of carbon-based polymer composites like Carbon Fibre-Reinforced Polymer (CFRP) Composites, Carbon Nanotubes (CNT) decorated by magnetic nanoparticles and graphene composites for stealth

✉ Suwarna Datar
suwarna.datar@gmail.com

Ramesh Kumar Mishra
rk.mishra1963@gmail.com

Ravi Dutt Gupta
ravidutt81@gmail.com

1 Department of Applied Physics, Defence Institute of Advanced Technology, Pune, MH 411025, India

2 Defence Institute of Advanced Technology, Pune, MH 411025, India

capability. They have been found to be flexible, strong and have shown very encouraging results. [10–12] However, control over operating bandwidth, homogeneity of inclusions and predictability of material properties poses some challenge. Also, production cost and difficulty in large-scale production and high weight penalty are few other challenges causing limitation of their applications for stealth capability against radars. Accordingly, thin, low weight, flexible metamaterials, designed as resonant structures, is a good alternative to these technologies. The objective of the present work is to study new designs of MMA suitable for application to the platform surfaces for stealth capability and EMI shielding applications in the X-band.

The first microwave absorbers using metamaterials were proposed and realised in 2008 by Landy et al. [7]. Many researchers have proposed different topologies and methodologies to produce high absorption of EM energy using them. This has been possible by reducing the reflection at the surface and by realising absorption of the waves in the intervening dielectric substrate by engineering the electrical and magnetic resonances to coincide at the same frequency.

EM wave absorbers have been engineered to operate at specific frequency spectrum ranging from microwave to ultraviolet with different features. They can be single band, multiband, broad band, polarisation insensitive, wide angle, etc. [13–16]. Metamaterial absorbers with switchable frequency [17] and wide band absorbers using Lumped components have also been reported [18, 19]. Amongst these, wide-angle metamaterial absorbers are most difficult to realise, particularly for the thin structures and they have been generally found to have maximum absorption for orthogonal incidence [20]. Increasing the angle of incidence has been seen to reduce the absorption characteristics considerably in most designs [21, 21–26]. The flexibility in realising metamaterial absorbers for various ranges of frequencies/wavelength, in the microwave region, in which most of the radars operate, makes them suitable candidate for designing and fabricating them to provide stealth capability to military targets against radars or in general as EMI shields. Such metamaterial absorbers in the microwave frequency domain shall be addressed as Metamaterial Microwave Absorber (MMA) in this paper.

Design of Basic Resonant MMA with Metal Back Plane

In the present work MMA structure with resonant design on a substrate having a metal back plane was chosen for investigation as shown in Fig. 1. The MMA design was conceived as a wheel with four spokes in a unit cell to provide inductive reactance loops in each quadrant and with cuts on the wheel in each quadrant to provide the capacitive element for the resonance. Annealed copper has been chosen for resonant ring and the back plane and lossy

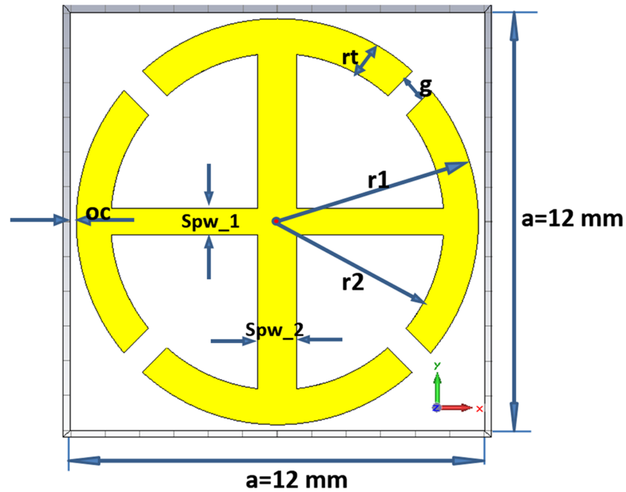

Fig. 1 Orthographic front view of the proposed MMA with spoke and wheel structure

FR-4 as the substrate. The thickness of the substrate is chosen as 0.6 mm which is sandwiched between annealed copper coatings of 0.035 mm on both sides. The resonant structure design can be screen printed and etched on one side and the other side is left as it is to provide the conducting back plane. The orthographic front view of the unit cell of proposed MMA is shown in Fig. 1 along with important design parameters where ‘a’ is cell size, ‘oc’ is outer clearance, ‘r1’ is outer radius of annular ring, ‘r2’ is inner radius, ‘rt’ is the ring width, ‘g’ is the capacitive gap, ‘spw_1’ is width of spoke 1 and ‘spw_2’ is width of spoke 2. The schematic arrangement of resonant structure, substrate and the back plane is shown in Fig. 2, with thickness represented as ‘st’ and conductor thickness ‘ct’ for resonant structure and the back plane. (The ct and st dimensions are exaggerated for visual understanding.)

Simulations were carried out on this MMA design in Frequency Domain using Computer Simulation Technologies Micro-Wave Studios (CST MWS) simulation software. Only Zmax port on the front side of design was used for excitation as shown in Fig. 3. The Zmin port on the opposite side was not used as no EM wave is expected to cross the continuous metallic back plane. This was done by putting electric field Et = 0 for the Zmin port in the boundary conditions.

The structure, being circularly symmetric, was expected to provide polarisation independence. [21] The small thickness of the substrate was expected to provide for the wide-angle performance. The structure being highly symmetric and resonant, when optimised, was expected to provide high absorption hence low reflection and low value of S-parameter at Zmax port (S_Zmax).

Further, to improve the bandwidth of absorption, 4-ring array structure was designed as shown in Fig. 4. The perspective

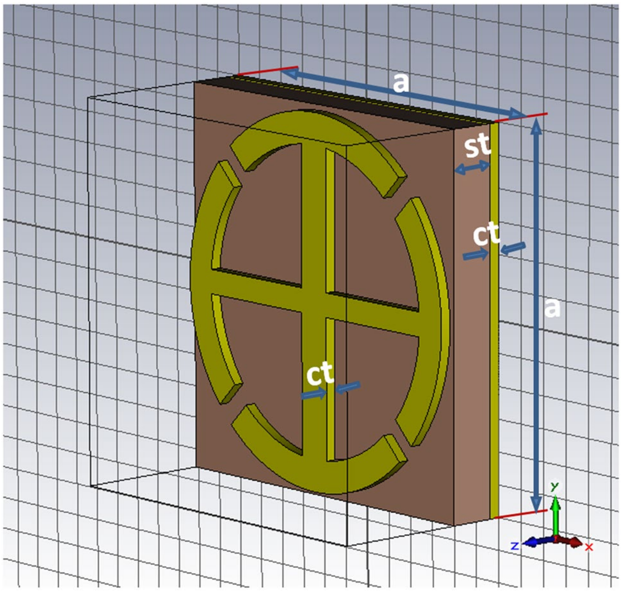

Fig. 2 Perspective schematic view of proposed MMA

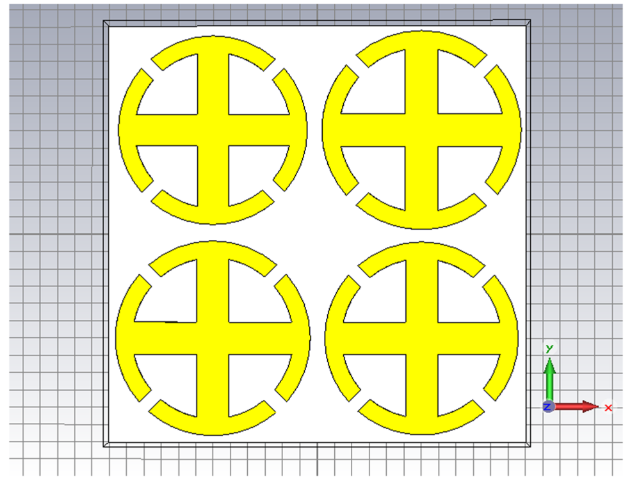

Fig. 4 The orthographic front view of the unit cell of 4-ring array-type spoke and cut-wheel MMA having each ring structure scaled in size using a scaling factor in X-Y plane

view of unit cell of the array is shown in Fig. 5. This structure has four resonant rings in each unit cell. The rings are scaled to different sizes in x-y domain to provide closely spaced peaks, thus increasing the operational bandwidth.

Simulation Results

MMA structures with plane annular rings without any cuts or a ring with a single cut were initially designed, simulated and optimised. It was found that the absorption increased when the spoke and cut-wheel structure was introduced (> 60 dB). It was also observed that, single cut structures or complementary ring structures are not symmetric with respect to rotation of electric field vector and hence do not exhibit good polarisation independence. In view of these preliminary observations during design and simulation steps, the spoke and cut-wheel structure was conceptualised and studied extensively.

The spoke and wheel MMA design was optimised using parametric sweeps during simulation, and the results with this MMA design showed very encouraging peak absorption. After optimisation, it gave ~100% absorption at the resonant frequency of 9.828 GHz with scattering parameter

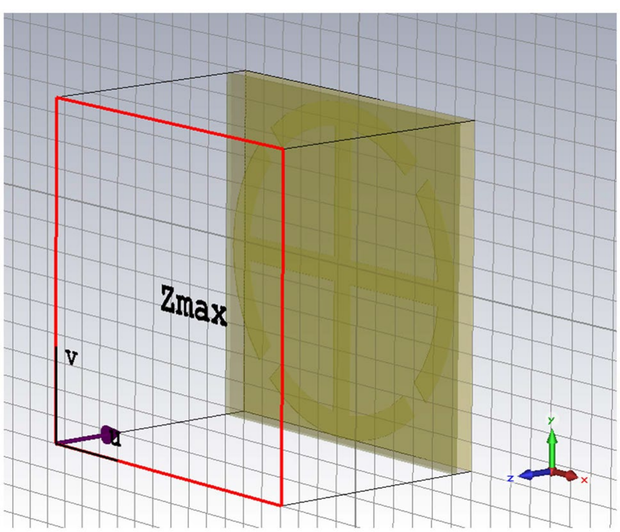

Fig. 3 Perspective view of Zmax port used for excitation. The Zmin port was not used because it is redundant due to metallic back plane

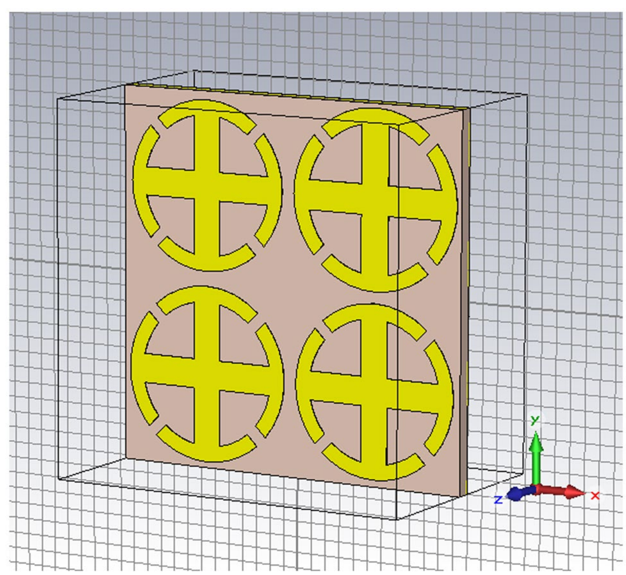

Fig. 5 The perspective view of the front side of unit cell of 4-ring array-type MMA

S_Zmax (depicting reflection back to the excitation port) as low as -65.97dB for normal incidence. Accordingly, it can be treated as perfect MMA for providing stealth capability at the design frequency.

From the Radar Range Equation, we know that the maximum range of radar is inversely proportional to the fourth root of minimum detectable Received Signal Level (RSL). [27] As the RSL will be reduced by ~66 dB at resonant frequency due to the MMA, the effective radar range will be reduced by a factor of approximately 40 times for the radar transmit frequency. This implies that, if MMA is designed for the radar transmit frequency, a monostatic/bistatic radar with a Maximum Detection Range of 400 km will be able to detect the target platform only when it has reached at a distance of approximately 10 km from the radar. This is very effective stealth capability. The attendant challenges here are the bandwidth, for different polarisation and direction of incidence of waves with respect to the MMA structure.

The simulation was done using Frequency Domain Solver of CST MWS simulation software, with smallest mesh size less than the smallest dimensions of the MMA. Option was chosen to get 10001 result data samples for a smooth graph and accuracy of simulation results. Other options were also chosen in a manner to present highest accuracy and correctness of simulation.

The simulation result for S_Zmax vs frequency for the optimised MMA is shown in Fig. 6. The total scattered EM energy from the structure, reaching back the excitation port (radar), is represented by S_Zmax and it has minima of -65.97 dB at the resonant frequency of 9.828 GHz and 10 dB bandwidth of approximately 154 MHz around it.

The FR-4 substrate thickness and conducting surface thickness were chosen as per specifications of commercially available standard materials in the market. The parameters

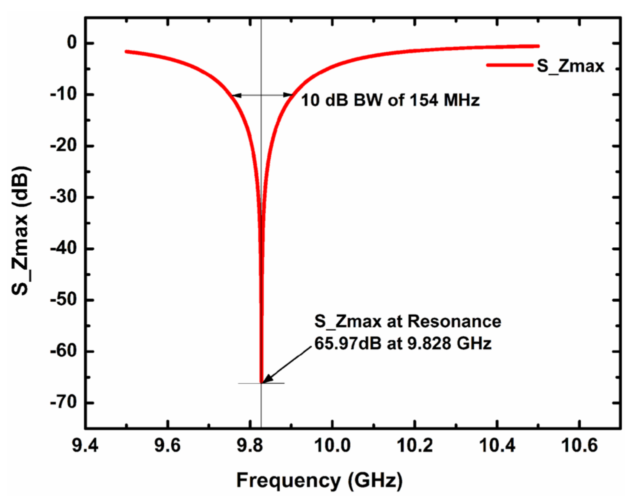

Fig. 6 Reflection parameter S_Zmax of -65.97 dB at normal incidence depicts 100% absorbance of scattered energy at the metasurface at resonant frequency

like outer clearance (oc), ring width (rt), gap width (g) and spoke widths (spw_1 and spw_2) were selected for optimisation to achieve better than -60dB values of S_Zmax at resonant frequency in the frequency range of 9.5 GHz to 10.5 GHz. The parameters of the optimised MMA structure are given in Table 1.

The design being symmetric to 90^0 rotation in X-Y plane was expected to exhibit polarisation independence. The dependence of absorbance on the polarisation angle Phi (ϕ) and the incidence angle Theta (θ) was studied by using Floquet mode excitation in the Frequency Domain Solver of the CST MWS by varying the spherical angle phi and theta in simulation. The orientation of spherical angles ϕ and θ is depicted in Fig. 7.

Simulations were carried out for the three cases that arise as given below:

For Changing Polarisation Angle ϕ while Keeping $\theta = 0^0$

Perfect polarisation independence was observed, as expected, due to 90^0 rotation symmetry of this MMA design. It can be seen from Fig. 8 that all the curves overlap, almost completely, over complete frequency range of simulation for all angles of polarisation.

For Changing Incidence Angle θ while Keeping ϕ=0^0

It was found that the maximum absorption was obtained at $\theta = 0^0$ at the resonant frequency of 9.828 GHz. However, in this case, the absorption gradually decreases with increasing incidence angle θ as shown in Fig. 9. S_Zmax was still better than -10 dB for incidence angle of 75^0 and -30 dB for $\theta = 45^0$. Thus, the acceptance cone angle is greater than 150^0 for 10 dB and 90^0 for 30dB of reduction

Table 1 The simulation parameters of the optimised spoke and cut-wheel (SCW) MMA

Sl. No.	Parameter	Optimised Parameter (in mm)	Description
1.	a	12.0	Cell size
2.	ct	0.035	Conductor thickness
3.	st	0.6	Substrate thickness
4.	oc	0.175	Outer clearance of ring
5.	rt	1.0	Ring width/thickness
6.	r1	5.825	Outer radius of ring
7.	r2	4.825	Inner radius of ring
8.	g	0.77	Capacitive gap width
9.	spw_1	0.76	Width of spoke pair 1
10.	spw_2	1.133	Width of spoke pair 2

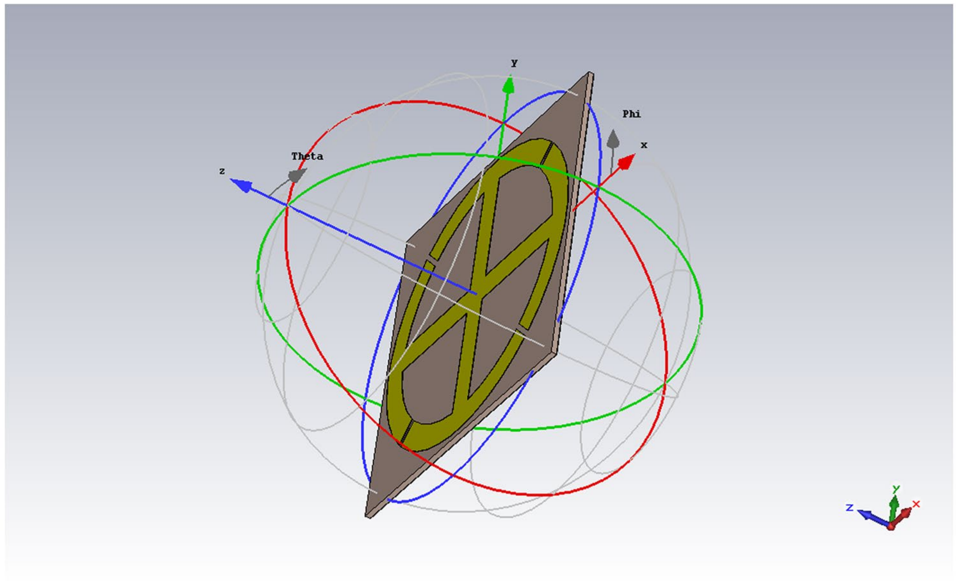

Fig. 7 Orientation of polarisation angle phi (ϕ) and incidence angle theta (θ). Angle ϕ varies along the blue circle and angle θ varies along the green circle

in RSL due to the MMA. There could be anomalous behaviour of MMA at very steep angles of incidence.

Both Polarisation Angle (ϕ) and Incidence Angle (θ) Varying (Keeping $\theta = \phi$)

When both polarisation and incidence angles are varied simultaneously, keeping them equal, very little change was observed in S_Zmax vs Frequency (Fig. 10) as compared to case of only incidence angle variation.

The biggest challenge with this perfect, but narrowband MMA conceived above was of increasing the operating bandwidth. It is known that the gain–bandwidth product of any resonant feedback system is generally constant. [28] Accordingly, it was expected that when the bandwidth is attempted to be increased, the gain (absorption in this case) is likely to suffer. The observations were as per expectations.

Many studies have been conducted on MMA structures to enhance the operating bandwidth by using the concept of stacking of multiple MMA layers. Here the resonant frequency-selective surfaces were separated by layers of substrate and were scaled up or down in size to resonate at closely spaced peak frequencies thus increasing resultant bandwidth. However, such multilayer structures have unacceptable weight penalty and possibility of peeling-off of the

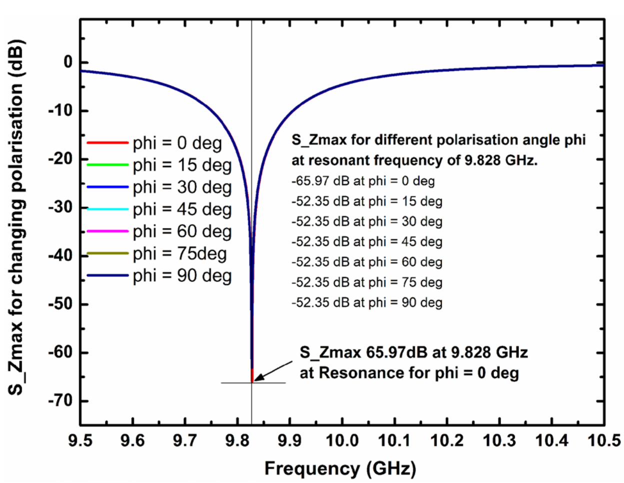

Fig. 8 S_Zmax vs frequency for varying polarisation angles ϕ while keeping $\theta = 0^0$

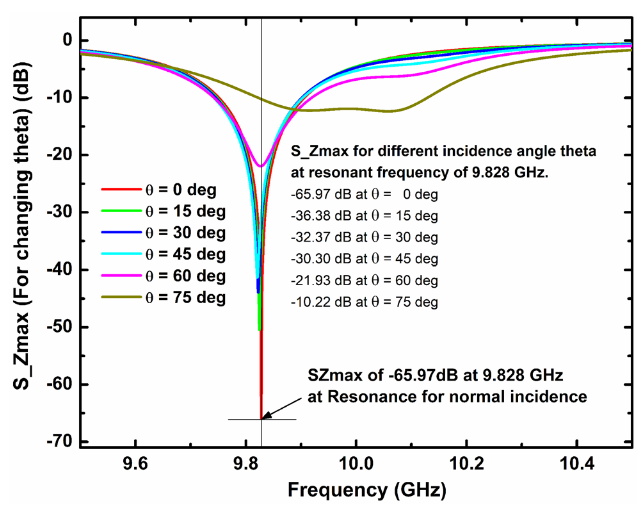

Fig. 9 S_Zmax vs frequency for varying incidence angles θ while keeping ϕ=0^0

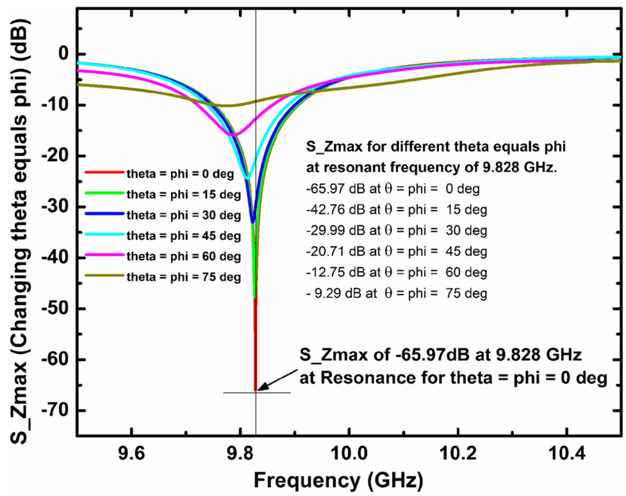

Fig. 10 S_Zmax vs frequency when both polarisation and incidence angle vary (keeping $\theta = \phi$)

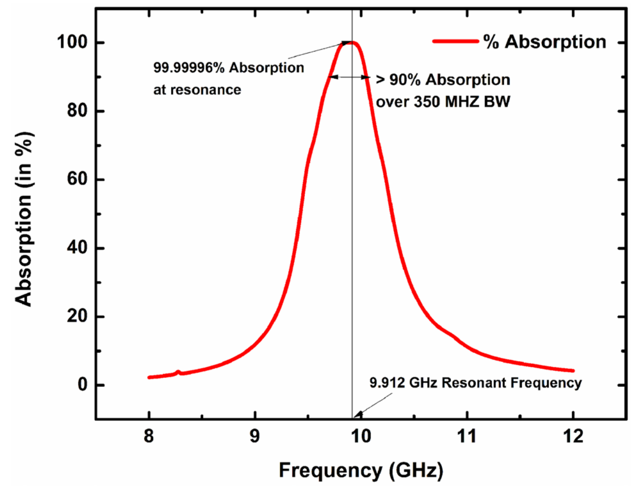

Fig. 11 Results of simulation on 4-ring planar array of spoke and cut-wheel MMA absorption vs frequency

layers from each other under thermal and other environmental stress. [21, 21–26]

The obvious solution is to keep the structure planar and single layer type, keeping the structure lighter and rugged. Thus, the scaling of resonant structures was to be done in the same plane itself. Accordingly, simulations on various planar-arrays were attempted, having more than one spoke and cut wheel structure, scaled in size, in the same X-Y plane only. The bandwidth enhancement was also attempted by changing the capacitive gaps in each quadrant of the ring. The results were encouraging for 2x2 Array of four rings.

The simulation and optimisation in time domain were carried out and minima of -63.8 dB was achieved for the S-parameter which is equivalent to absorbance of 99.99996% at 9.912 GHz. It showed an enhancement of bandwidth by 3 to 8 times as compared to the sharply resonant peak of single-ring single-layer MMA structure as seen in Fig. 6 above. The results of 4-ring array for absorption and S-parameter with increased bandwidth are shown in Figs. 11 and 12, respectively. It shows a 30 dB bandwidth of Approximately 96 MHz.

To explore the mechanism of TE (0,0) mode EM wave absorption by the structure, surface current density distributions pattern on top and bottom metallic layers was studied on-resonance (9.828 GHz) and off-resonance (8GHz) using field monitors. Figure 13 shows the current density distribution at top and at bottom metal surfaces at frequency 8 GHz (a), (b)) and 9.828 GHz ((c), (d)), respectively. While for both the frequencies one can see that the current is mostly concentrated on the structure shape for the top metal surface, it is weak and distributed at the bottom plane indicating absorption in the intervening lossy FR-4 substrate. The direction of surface current on top layer is anti-parallel with respect to that at the backplane, which results in equivalent current loops within the MMA that excites a magnetic dipole. Further, the surface current in the two arms at the end of the vertical spoke is also anti-parallel to each other, thus functioning as a dipole completing the loop inside the structure through the substrate and resulting in strong absorption. It is further observed that the surface currents are not anti-parallel in the other spoke and arms thus not forming resonant dipoles and loops. The localisation of incident energy of EM wave at resonance at the opposite end of spokes and beneath it on the backplane indicates formation of strong dipoles. Furthermore, when top planes and bottom planes of the

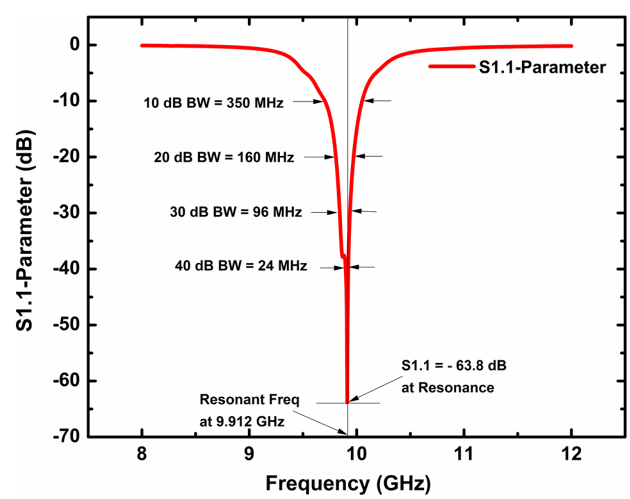

Fig. 12 Results of simulation on 4-ring planar array of spoke and cut-wheel MMA S1.1 parameter vs frequency

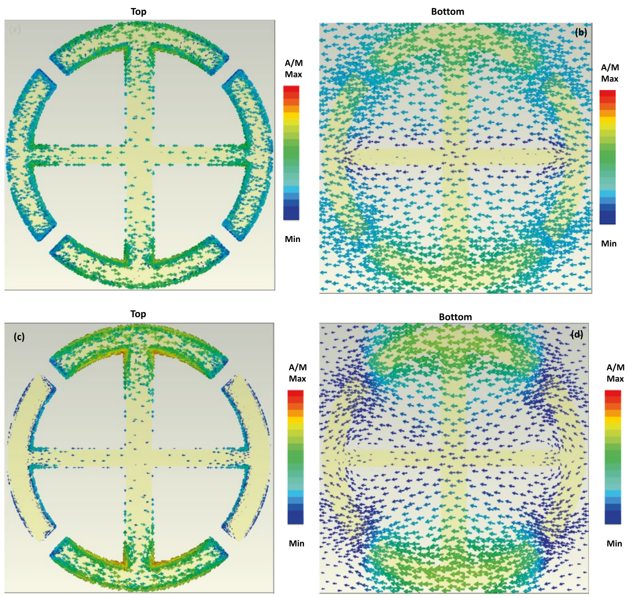

Fig. 13 Figure 13 **(a)**, **(b)** Surface current distribution at off-resonant frequency at 8.0 GHz and **(c)**, **(d)** on-resonance at 9.828 for top and bottom plane for the normally incident, plane-polarised EM waves in TE (0,0) mode

two frequencies are compared, current seems to be mostly concentrated on the vertical axis at resonance while it is uniformly distributed off resonance. The maximum surface current in the structure at 8.0 GHz is 195.5 A/m only as compared to the peak surface current of 2057 A/m at the resonant frequency of 9.828 GHz, thus having ratio of approximately 1:10 between the two.

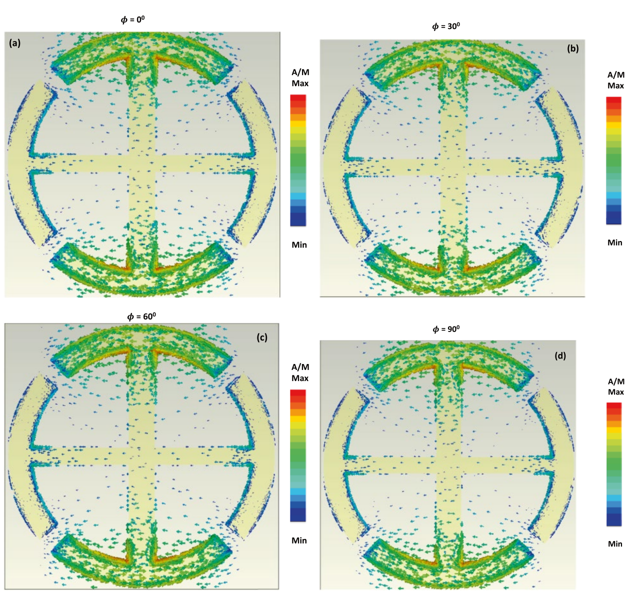

Fig. 14 Figure 14 **(a)**, **(b)**, **(c)**, **(d)** For the normally incident, plane-polarised EM waves in TE (0,0) mode, by changing the polarisation angle *phi* from 0 to 90° shows similar peak values and distribution pattern in all four cases, depicting polarisation independence of proposed MMA structure

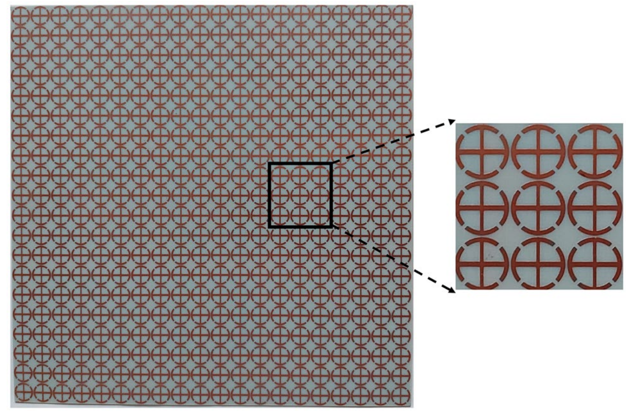

Fig. 15 Photograph of 20 x 20 array of fabricated MMA measuring 240 mm x 240 mm and expanded view on the right side

To further explore the polarisation independence characteristics of the proposed MMA, surface current distribution at resonance frequency in the structure was investigated through simulations carried out by varying polarisation angle (*phi*) for TE (0,0) mode. The simulation results shown in Figs. 8 and 14 clearly show that the absorption remains essentially same as the resonance characteristics of this MMA structure do not alter much with changing polarisation from 0 to 90°.

Fabrication and Testing

A spoke and cut-wheel MMA was fabricated by using FR-4 as substrate and copper as conductor by creating a mask using gerber (.gbr) format of design from CST MWS

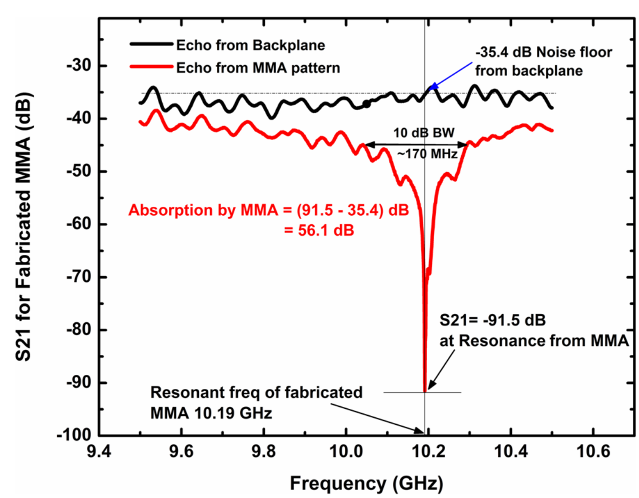

Fig. 16 Results of testing of single ring spoke and cut-wheel MMA structure

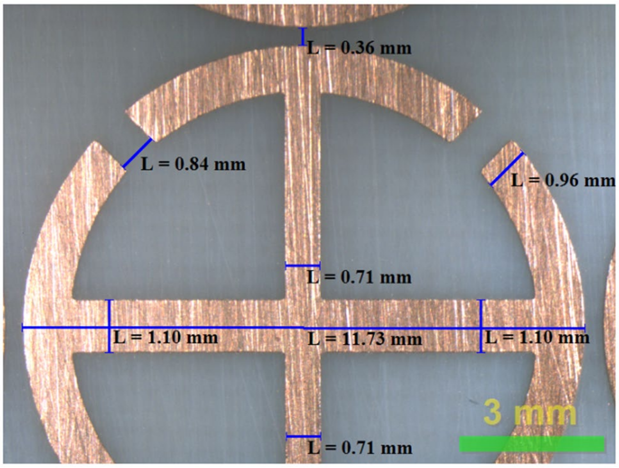

Fig. 17 Measurements carried out on the fabricated MMA using microscope

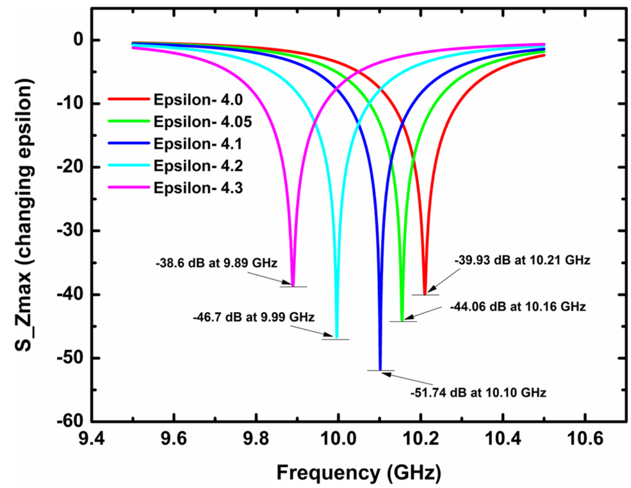

Fig. 18 Simulations carried out using measurements of the parameters of fabricated MMA while changing the electrical permittivity (Epsilon) of the FR-4 substrate

software and then using photo-printing and etching technique to remove the remaining copper as shown in Fig. 15.

The testing of the fabricated MMA was carried out by first subjecting the back plane side of the MMA to RF wave around the resonant frequency in the X-Band. The microwaves were generated and transmitted by an RF source (Vector Network Analyser) and transmitting antenna and then received at an antenna located adjacent to it. This served as the reference graph representing the echo from a metallic platform of interest without the MMA pasted over it and the random noise reflections from the surroundings as shown in black colour in Fig. 16 for the given set-up. The frequency sweep was narrowed down around the resonant frequency for better appreciation of BW. Keeping the set-up and the environment exactly same, the MMA was flipped and the resonant structure was exposed to the incident EM waves. The resulting signal received at the receiving antenna represented the EM wave after absorption by the MMA across the swept frequency range as seen in red colour in Fig. 16.

The comparison of S21 curves for the reference plane and from the resonant surface represents the absorption by the MMA. Absorption of 56.1 dB was observed at the resonant frequency of 10.19 GHz for this fabricated MMA which was higher than the resonant frequency of 9.828 GHz as predicted in the simulations. This is possibly due to material and fabrication tolerances. However, it validated the high absorbance possible with the spoke and cut-wheel design of the MMA. To identify the cause of reduction in absorption properties of structure and the shift in resonant frequency, measurements were carried out on the fabricated MMA using microscope. The measured parameters (as shown in Fig. 17) were not exactly as per the gerber file given for the designed MMA with the design parameters as mentioned in Table 1.

Simulation was then carried out on the MMA design with the parameters measured on the fabricated MMA. Minor drift in resonant frequency towards the measured resonant frequency was observed indicating fabrication and material tolerance causing the drift. Further, any changes in the orthogonality of the incident radiation also cause shift in resonant frequency as can be seen from Fig. 9. However, it did not explain the large change in resonant frequency of the order of 300 MHz to 400 MHz. The parameters of the material used were suspected and the epsilon value (electric permittivity) of the substrate was varied in simulations. The observations easily explain the drift in resonant frequency for the fabricated MMA. These simulation results for the fabricated MMA, as per measured parameters and changing epsilon, predicted epsilon ~4.1 for the material used for fabrication instead of 4.3 as available in CST MWS Library of materials.

Results obtained during experiments with fabricated MMA (absorption 56.1 dB at 10.19 GHz) were closest for simulation carried out with epsilon equals to 4.1 (absorption ~51.74 dB at 10.10 GHz) as seen in Fig. 18. It indicates that the FR-4 material used for fabrication has epsilon value of ~4.1 instead of the value of 4.3 used during optimisation of design.

Table 2 Performance comparison between the proposed MM absorber and previously reported MMAs

Sl. No.	Features	10 dB BW and Peak Absn	40 dB BW	Polsn Indep	Wide Angle Performance	Thickness and Flexibility	Remarks
1.	Multilayer structure, wide band, poln insensitive [29].	2.3 GHz to 18.9 GHz, ~20 dB absn.	Nil	Yes	Not reported.	11 mm, Not flexible.	Thick, multilayer structure, not suitable for aircraft.
2.	Two layered hybrid absorbers with epoxy loaded foam. Good results with 13 mm thickness [30].	2 GHz to 18 GHz, and ~20 dB absn.	Nil	Yes	Shift in peak absn freq with changing angle hence reduced absn at fixed freq.	13 mm, Not flexible.	13 mm thick, double layer structure, not suitable for stealth aircraft.
3.	Split circular and square rings configuration. BW improved by changing section lengths [22].	12.8 GHz to 16.6 GHz, and ~20 dB absn.	Nil	Highly sensitive to polsn.	Shift in peak absn freq with changing angle hence reduced absn at fixed freq.	1.0 mm, Flexible.	Polsn and incidence angle dependence. Absorptivity of only, ~10 dB across BW.
4.	Single layer, Annular Ring with a split subtending an angle at centre [31].	5.94 GHz to 16.84 GHz, and ~30 dB absn.	Nil	No	Absn drops drastically with changing incidence angle, < 70% at 15^0.	4mm, Not flexible.	Thick, polsn and incidence angle sensitivity. Not suitable for stealth.
5.	Periodic array of metal-dielectric. multilayered frustum pyramids [32].	1 GHz to 15 GHz and ~15 dB absn.	Nil	Yes	Good up to 40^0 Absorption suffers after 60^0 and becomes < 80%	5mm, Not flexible.	5mm thick pyramidal structures are not suitable for stealth aircraft.
6.	Multilayered structure using lumped resistors, Multiband resonance. Large BW [23].	Aim Appears to be large BW only ~30 dB absn.	Nil	Fair	Incidence angle changes peak absn freq as well as the absn.	5mm, Not flexible.	Not suitable for stealth aircraft needs to be thinner and flexible.
7.	Single layer Two scaled elements per cell for wider BW [24]. [24]	FWHM BW GHz 4.97- 5.55 GHz and ~30 dB absn.	Nil	Yes	Reasonable up to 30^0. Drops thereafter.	1.6 mm, Not enough flexible.	Not suitable for stealth aircraft needs to be thinner and flexible.
8.	Asymmetric structure at two corners [25].	10.45 GHz to 17.64 GHz ~26 dB absn.	Nil	No	No. Sensitive to incidence angle.	1.6 mm, Not enough flexible.	Not suitable for stealth aircraft.
9.	Thin, Single Layer. Three designs, one for each peak of ~30 dB absn [21].	BW in MHz at resonant peaks and ~30 dB absn.	Nil	yes	Incidence angle changes peak absn freq as well as the absn.	0.4 mm, hence flexible.	Complicated design. Peak absn could be higher.
10.	Detailed comparison of latest Narrow-Band and Wide-Band MMA [20].	All designs reporting < 30 dB absn.	Nil	yes	Wider BW through Lumped resistors. Not suitable for aircrafts	discussed structures are flexible.	All structures report < 30 dB. Peak absn.
11.	Single layer, Hybrid structure. Uses resistors for wider BW [26].	7 GHz to 12.8 GHz and ~30 dB absn.	Nil	Good	Good	3.4 mm Not flexible.	Thick, not flexible, lumped resistors. Make it not suitable for stealth aircraft.
12.	Single layer, resonant, circularly symmetric, light weight, flexible, polsn indep, wide-angle performance. Extreme Absn ~64dB not reported in literature. BW increased	350 MHz at resonant freq for scaled co-planar 2X2 array in the unit cell. 99.99996% or	24 MHz at 9.91 GHz (resonant freq).	Excellent due to circular symmetry. > 52 dB absn for all angles	Excellent absn (99.9%) up to 30^0 angle of incidence > 90% absn even at 75^0 of incidence angle for all polsn.	0.6 mm hence flexible. only challenge is 10dB BW improvement.	Reduction in Max radar range is nearly 40 times on at resonant freq. Suitable for Stealth aircraft application due to

Table 2 (continued)

Sl. No.	Features	10 dB BW and Peak Absn	40 dB BW	Polsn Indep	Wide Angle Performance	Thickness and Flexibility	Remarks
	by scaling in same plane.	~64 dB absn.		of polsn.			reported features.
	[This Work]	~64 dB absn.		of polsn.			reported features.
	Abbreviations Used- absn: absorption; polsn: polarisation; indep: independence;						

Conclusions

Presented work consists of conceiving and simulating a perfect Metamaterial Microwave Absorber (MMA) with extremely high absorbance over a fairly wide band in the X-Band while exhibiting polarisation independence and wide-angle performance. It was also aimed to keep the structure light and flexible for which it was kept as a single-layer planar array in a unit cell over a thin FR-4 substrate of 0.6 mm. The optimisation of the conceived spoke and cut-wheel structure of the MMA showed excellent absorption results of 99.99996% absorbance (and S-parameter of –65.97 dB) at resonance frequency of 9.828 GHz and 10 dB BW of 150 MHz around resonance. Widening of bandwidth was achieved by creating a unit cell having a planar array of 4 rings scaled to different sizes in such a way so as to keep the resonance frequency of each ring close by to each other. This structure when optimised gave a resonant peak absorption of 63.8 dB at 9.912 GHz and bandwidth enhanced by 3-8 times as compared to bandwidth presented by the structure having single ring per unit cell. The extremely high absorption results of greater than 66 dB achieved in simulation and duly validated by experiments have not been reported earlier while simultaneously exhibiting the other features of light weight, flexibility, polarisation independence and wide-angle performance with reasonable bandwidth in X-Band.

The features of the presented work and the results obtained have been compared against various parameters, after extensive survey, to other similar works reported in the recent past. These are brought out in Table 2. It has been found in the survey that even the narrow-band MMAs have not reported with absorption peaks greater than 40 dB, while simultaneously achieving perfect polarisation independence and excellent wide-angle performance. These features, coupled with light weight and flexibility, make it a suitable candidate for application on aircraft for stealth capability against radars. The proposed design of MMA can also be used for excellent EMI shielding of own resources against known frequencies. For example, it can be used for shielding receiver against own and other transmitter radiation while maintaining nearly transparent window. The only challenge of increasing the bandwidth, while maintaining other features, is a subject of further study.

Author Contributions R. K. Mishra performed simulation, validation, formal analysis and writing—original draft. R. D. Gupta performed simulation. S. Datar contributed to conceptualisation, formal analysis, writing—review and editing, and funding acquisition.

Funding Information Authors would like to acknowledge the funding and support from Defence Institute of Advanced Technology, Pune, and testing facility at Armament Research and Development Establishment, Pune.

Data Availability Statement The data that support the findings of this study are available from the corresponding author upon request.

Code Availability The simulation code that supports the findings of this study is available from the corresponding author upon request.

Declarations

Consent to Participate Informed consent was obtained from all authors.

Consent for Publication The authors confirm that there is informed consent to the publication of the data contained in the article.

Conflicts of Interest There are no conflicts to declare.

References

1. Veselago V (2002) Electrodynamics of media with simultaneously negative electric permittivity and magnetic permeability. In Advances in electromagnetics of complex media and metamaterials. Springer, pp. 83–97
2. Caloz C, Itoh T (2006) Metamaterials: Transmission line theory and microwave applications: The engineering approach. A John Willy & Sons Inc., Publication
3. Cui TJ, Smith DR, Liu R (2010) Metamaterials. Springer
4. Liu R, Ji C, Mock J, Chin J, Cui T, Smith D (2009) Broadband ground-plane cloak. Science 323(5912):366–369
5. Schurig D, Mock JJ, Justice B, Cummer SA, Pendry JB, Starr AF, Smith DR (2006) Metamaterial electromagnetic cloak at microwave frequencies. Science 314(5801):977–980
6. Fang N, Lee H, Sun C, Zhang X (2005) Sub-diffraction-limited optical imaging with a silver superlens. Science 308(5721):534–537

7. Landy NI, Sajuyigbe S, Mock JJ, Smith DR, Padilla WJ (2008) Perfect metamaterial absorber. Phys Rev Lett 100(20):207402
8. Zhi Cheng Y, Wang Y, Nie Y, Zhou Gong R, Xiong X, Wang X (2012) Design, fabrication and measurement of a broadband polarization-insensitive metamaterial absorber based on lumped elements. J Appl Phys 111(4):044902
9. Li H, Yuan LH, Zhou B, Shen XP, Cheng Q, Cui TJ (2011) Ultrathin multiband gigahertz metamaterial absorbers. J Appl Phys 110(1):014909
10. Chen Z, Xu C, Ma C, Ren W, Cheng HM (2013) Lightweight and flexible graphene foam composites for high-performance electromagnetic interference shielding. Adv Mat 25(9):1296–1300
11. Qi X, Xu J, Hu Q, Deng Y, Xie R, Jiang Y, Zhong W, Du Y (2016) Metal-free carbon nanotubes: synthesis, and enhanced intrinsic microwave absorption properties. Sci Rep 6:28310
12. Joshi A, Bajaj A, Singh R, Anand A, Alegaonkar P, Datar S (2015) Processing of graphene nanoribbon based hybrid composite for electromagnetic shielding. Composites Part B: Eng 69:472–477
13. Pendry JB, Holden AJ, Robbins DJ, Stewart W (1999) Magnetism from conductors and enhanced nonlinear phenomena. IEEE Trans Micro Theo Tech 47(11):2075–2084
14. Smith DR, Padilla WJ, Vier D, Nemat-Nasser SC, Schultz S (2000) Composite medium with simultaneously negative permeability and permittivity. Phys Rev Lett 84(18):4184
15. Xiong H, Zhong LL, Luo CM, Hong JS (2015) Dual-band polarization-/angle-insensitive metamaterial absorber. Aip Adv 5(6):067162
16. Li L, Yang Y, Liang C (2011) A wide-angle polarization-insensitive ultra-thin metamaterial absorber with three resonant modes. J Appl Phys 110(6):063702
17. Li W, Zhou X, Ying Y, Qiao X, Qin F, Li Q, Che S (2015) Polarization-insensitive wide-angle multiband metamaterial absorber with a double-layer modified electric ring resonator array. AIP Adv 5(6):067151
18. Shen X, Cui TJ, Zhao J, Ma HF, Jiang WX, Li H (2011) Polarization-independent wide-angle triple-band metamaterial absorber. Opt Exp 19(10):9401–9407
19. Ling K, Kim HK, Yoo M, Lim S (2015) Frequency-switchable metamaterial absorber injecting eutectic gallium-indium (egain) liquid metal alloy. Sensors 15(11):28154–28165
20. Ghosh S, Nguyen TT, Lim S (2019) Recent progress in angle-insensitive narrowband and broadband metamaterial absorbers. EPJ Appl Metamaterials 6:12
21. Deng G, Lv K, Sun H, Yang J, Yin Z, Li Y, Chi B, Li X (2020) An ultrathin, triple-band metamaterial absorber with wide-incident-angle stability for conformal applications at x and ku frequency band. Nanoscale Res Lett 15(1):1–10
22. Ramya S, Srinivasa Rao I (2018) An ultra-thin compact wideband metamaterial absorber. Radioengineering 27(2):364–372
23. Li SJ, Wu PX, Xu HX, Zhou YL, Cao XY, Han JF, Zhang C, Yang HH, Zhang Z (2018) Ultra-wideband and polarization-insensitive perfect absorber using multilayer metamaterials, lumped resistors, and strong coupling effects. Nanoscale Res Lett 13(1):386
24. Mol VL, Aanandan C (2017) An ultrathin microwave metamaterial absorber with enhanced bandwidth and angular stability. J Phys Comm 1(1):015003
25. Sood D, Tripathi CC (2017) A compact ultrathin ultra-wideband metamaterial microwave absorber. J Microwaves, Optoelec Electromag Appl 16(2):514–528
26. Nguyen TT, Lim S (2018) Angle-and polarization-insensitive broadband metamaterial absorber using resistive fan-shaped resonators. Appl Phys Lett 112(2):021605
27. Skolnik MI, et al (1980) Introduction to radar systems, vol. 3. McGraw-hill New York
28. Gilbert B, Toumazou C, Moschytz GS (2002) Trade-offs in Analog Circuit Design: The Designer's Companion. Kluwer Academic
29. Deng G, Lv K, Sun H, Hong Y, Zhang X, Yin Z, Li Y, Yang J (2020) An ultra-wideband, polarization insensitive metamaterial absorber based on multiple resistive film layers with wide-incident-angle stability. Int J Microwave Wireless Techn, 1–9
30. El Assal A, Breiss H, Benzerga R, Sharaiha A, Jrad A, Harmouch A (2020) Toward an ultra-wideband hybrid metamaterial based microwave absorber. Micromachines 11(10):930
31. Bhattacharyya S, Ghosh S, Srivastva KV (2016) A microwave metamaterial absorber with wide bandwidth. In 2016 URSI Asia-Pacific Radio Science Conference (URSI AP-RASC, IEEE, pp. 1215–1218
32. Ding F, Cui Y, Ge X, Jin Y, He S (2012) Ultra-broadband microwave metamaterial absorber. Appl Phys Lett 100(10):103506